Microstructure and Mechanical Properties of Ultrafine-Grained Copper Produced Using Intermittent Ultrasonic-Assisted Equal-Channel Angular Pressing

JIANXUN LU, XIAOYU WU, ZHIYUAN LIU, XIAOQIANG CHEN, BIN XU, ZHAOZHI WU, and SHUANGCHEN RUAN

We proposed intermittent ultrasonic-assisted equal-channel angular pressing (IU-ECAP) and used it to produce ultrafine-grained copper. The main aim of this work was to investigate the microstructure and mechanical properties of copper processed by IU-ECAP. We performed experiments with two groups of specimens: group 1 used conventional ECAP, and group 2 combined ECAP with intermittent ultrasonic vibration. The extrusion forces, microstructure, mechanical properties, and thermal stability of the two groups were compared. It was revealed that more homogeneous microstructure with smaller grains could be obtained by IU-ECAP compared with copper obtained using the traditional ECAP method. Mechanical testing showed that IU-ECAP significantly reduced the extrusion force and increased both the hardness and ultimate tensile stress owing to the higher dislocation density and smaller grains. IU-ECAP promotes conversion from low-angle grain boundaries to high-angle grain boundaries, and it increases the fractions of subgrains and dynamic recrystallized grains. Group 2 statically recrystallized at a higher temperature or longer duration than group 1, showing that group 2 had better thermal stability.

I. INTRODUCTION

EQUAL-CHANNEL angular pressing (ECAP) is a severe plastic deformation technique used to refine grain size of a material without changing its shape. The strength of a material improves as grain size decreases in accordance with the Hall–Petch effect.[1,2] In conventional polycrystalline materials, grain boundaries can effectively block dislocation motion, necessitating a stronger external stress to drive the slip deformation. Many researchers have made further contributions to the development of the technique since Segal[3] invented ECAP in 1977. For example, Valiev et al.[4] and Langdon[5] investigated the principles of grain refinement. Cetlin et al.[6] discussed how to avoid cracks and inhomogeneities in billets processed by ECAP. Some methods were proposed to assist the ECAP technique to improve the properties of materials. It was reported that back-pressure could prevent the fracture of low ductile materials during ECAP.[7] In addition, a beveled-edge punch was introduced to improve the homogeneity of ultrafine-grained materials.[8] Furthermore, ECAP was used to combine with other processes. Zhilyaev et al.[9] reported the evolution of microstructure and microtexture in ultrafine-grained materials by ECAP combined with HPT (high-pressure torsion). Recently, ECAP was used to improve the performance of various metallic materials, including aluminum, copper, titanium, low carbon steel, nickel, and many alloys.[10–15] However, there are still many flaws during ECAP, such as large extrusion force, heterogeneous grain sizes, poor thermal stability, which needs to be further ameliorated.

Ultrasonic-assisted plastic processing has been applied to metal forming processes since the 1960s. Comprehensive studies of this method have been performed. It was reported that Huang et al.[16] found that ultrasonic vibration decreases the forming load and improves the friction condition with increases in temperature. Liu et al.[17] also revealed that ultrasonic vibration can heat a specimen to about 507 K (234 °C). Furthermore, Pal et al.[18] and Zhang et al.[19] illustrated that ultrasonic vibration can increase dislocation density. Ahmadi et al.[20] and Djavanroodi et al.[21] experimented with combining ECAP and ultrasonic vibration for use in pure Al. Ahmadi et al.[22] further investigated how ultrasonic excitation affected pure aluminum specimens with various grain sizes in tensile tests. However,

JIANXUN LU and ZHAOZHI WU, Ph.D. Students, XIAOQIANG CHEN, Undergraduate Student, BIN XU, Assistant Professor, XIAOYU WU, Professor, and ZHIYUAN LIU, Associate Professor, are with the Guangdong Provincial Key Laboratory of Micro/Nano Optomechatronics Engineering, Shenzhen University, Nanhai Ave 3688, Shenzhen 518060, Guangdong, P.R. China and also with the Shenzhen Key Laboratory of Advanced Manufacturing Technology for Mold & Die, Shenzhen University, Nanhai Ave 3688, Shenzhen 518060, Guangdong, P.R. China. Contact e-mail: wuxy@szu.edu.cn, zyliu@szu.edu.cn SHUANGCHEN RUAN, Professor, is with the Guangdong Provincial Key Laboratory of Micro/Nano Optomechatronics Engineering, Shenzhen University.
Manuscript submitted January 20, 2016.
Article published online June 30, 2016.

all these studies used continuous ultrasonic vibration, while intermittent ultrasonic vibration has been studied little. Ultrasonic vibration can heat a specimen, known as the thermal effect, which can eventually cause grain growth and decrease material strength. As such, the thermal effect of ultrasonic vibration must be strictly controlled.

To address this issue, we propose the intermittent ultrasonic-assisted equal-channel angular pressing (IU-E-CAP) technique and use it to produce ultrafine-grained copper in this work. IU-ECAP controls the thermal effect of ultrasonic vibration by adjusting the ultrasonic exposure time. The main aim of this work is to investigate the microstructure and mechanical properties of copper processed by IU-ECAP and to reveal the differences between conventional ECAP and IU-ECAP.

II. EXPERIMENTAL PROCEDURE

A 99.96 pct cold-drawn copper bar with an average grain size of 15 μm (Figure 1) was used, its ingredients are detailed in Table I. The as-received copper bar was machined into cylinder specimens first, each with a diameter of 3 mm and length of 10 mm. Then the specimens were divided into the two groups: specimens in group 1 underwent conventional ECAP, while specimens in group 2 experienced intermittent ultrasonic vibration during ECAP. To investigate the effect of intermitten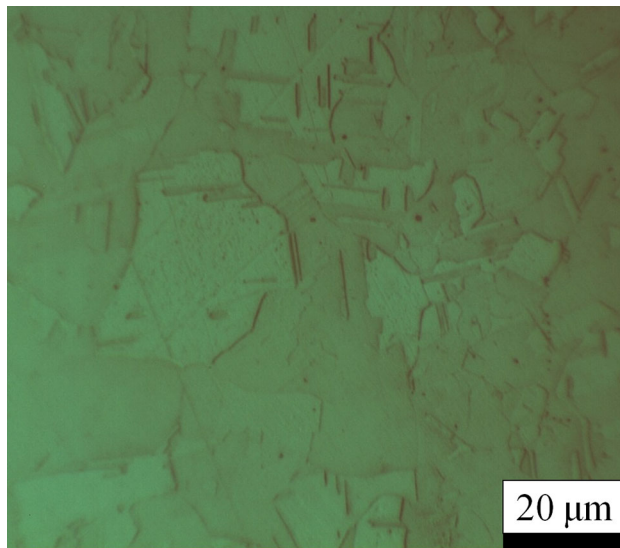t ultrasonic vibration during ECAP, we performed the two groups of experiments for eight passes, respectively, at room temperature following route Bc. Route Bc is defined as a 90 deg rotation of the workpiece in the same direction between each ECAP extrusion.[4]

Figure 2(a) shows the schematic and the axis reference system of the pressing channel, where x, y, and z were the extrusion direction, vertical direction, and horizontal direction, respectively. The equivalent
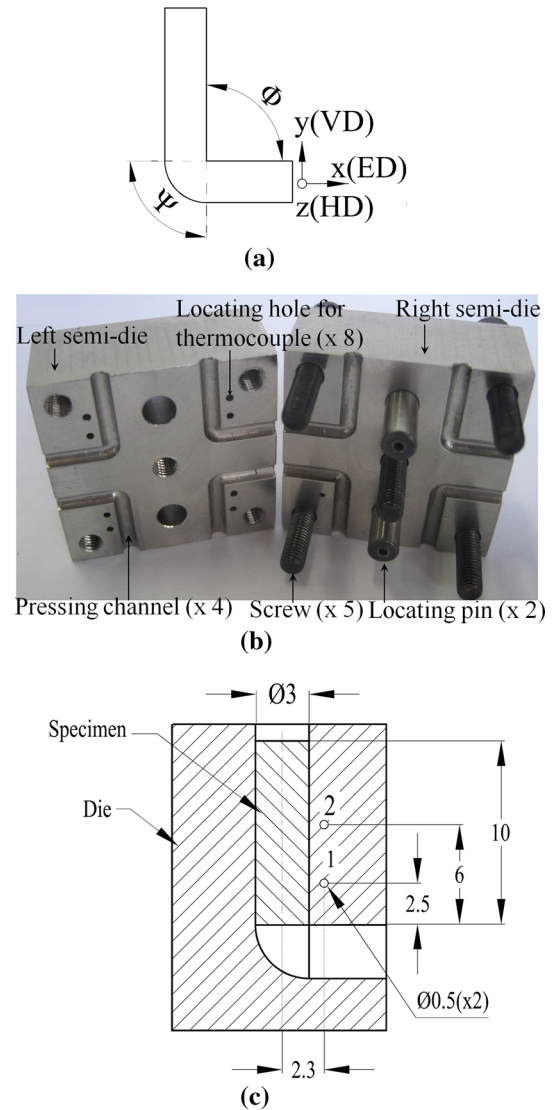
(a)

(b)

(c)

Fig. 2—Extrusion die: (*a*) schematic and the axis reference system of the pressing channel, (*b*) photo of extrusion die, (*c*) the detailed structure for temperature measurement.

Fig. 1—Optical micrograph of as-received copper.

Table I. Chemical Composition of the Pure Copper

Element	Wt Pct	Element	Wt Pct	Element	Wt Pct	Element	Wt Pct
Cu	99.96	P	0.0007	Ni	0.0002	Si	0.0004
Fe	0.0008	Zn	0.0009	Pb	0.0001	Sn	0.0001
S	0.0009	Ag	0.0010				
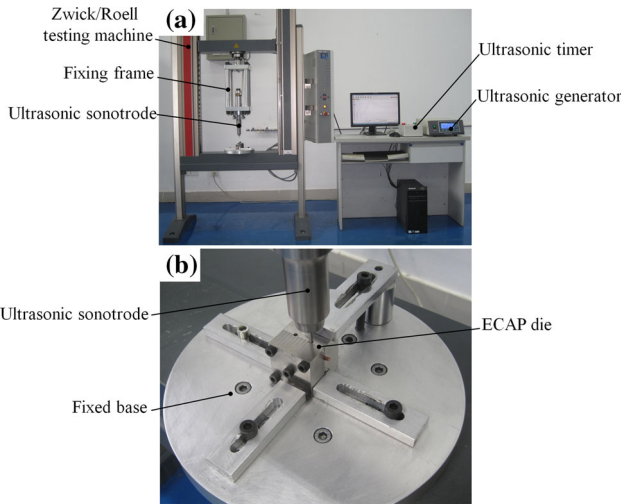
Fig. 3—Experimental setup: (a) related equipments, (b) the main working parts.

Fig. 4—Extrusion force: (a) extrusion force of the two groups, (b) load and deformation of both groups at the 8th pass, (c) square-wave analysis.

strain of each pass was ~0.91, following Iwahashi's relationship.[23]

Figure 2(b) shows the extrusion die with four optional pressing channels, a single channel with an inner angle (Φ), and an outer angle (Ψ) of 90 deg. Because ultrasonic vibration could cause die wear, four optional pressing channels would improve the utilization rate of the extrusion die. The die was made of SKD11, and constructed from two separate components by CNC machining that were then bolted together.

Figure 2(c) shows the detailed structure for temperature measurement. In order to monitor the temperature change of the die strictly, the temperature was measured at the two locations of holes 1 and 2, respectively. The two holes were respectively used to fix the thermocouple that was connected with a temperature measurement system (NI 9213). This system could collect 1000 temperature data within 10 seconds. Then the heat absorbed by the die could be evaluated based on the temperature change. This analysis presumes that the heat absorbed by the die equals to the heat released by the specimen in general. Therefore, the temperature change of specimens could be calculated.

Figure 3(a) shows the experimental setup: a tensile machine (Z050, Zwick/Roell, Germany), a 2-kW ultrasonic generator operating at a frequency of 20 kHz and amplitude of 5 μm, an ultrasonic timer, an ultrasonic sonotrode, a fixing frame, an extrusion die, and a fixed base. Figure 3(b) shows that the main working parts of the ultrasonic sonotrode and the extrusion die. The ultrasonic timer was used to control the ultrasonic exposure time in group 2, while the ultrasonic generator and timer were turned off in group 1. Because of its thermal effect, continuous ultrasonic vibration has the potential to soften and partially melt the copper specimen. To avoid this, after many tests we set up the IU-ECAP to suspend the ultrasonic exposure for 4 seconds after every 4 seconds of exposure. The extrusion speed was 0.05 mm/s, and the extrusion processes used no lubricating fluid.
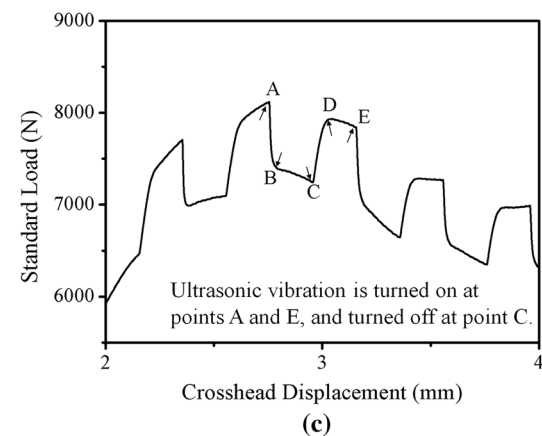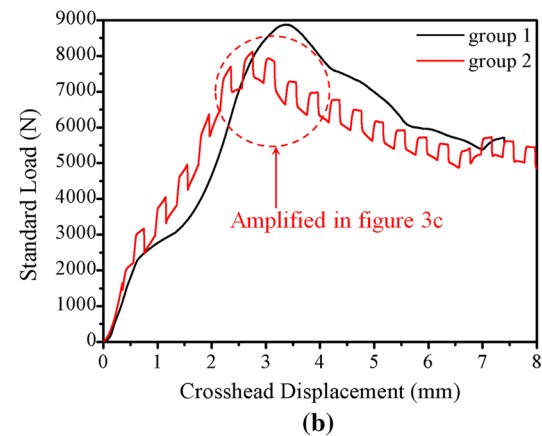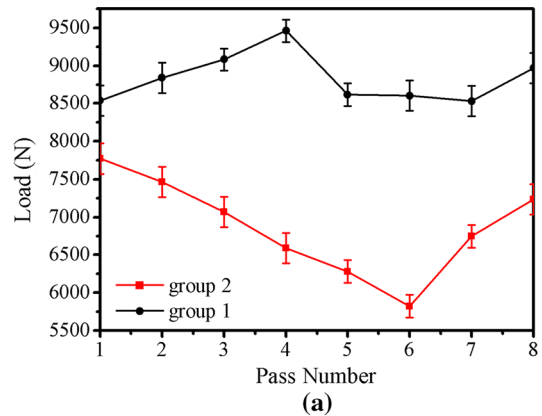
The microstructure of the specimens was characterized by electron backscatter diffraction (EBSD) on the longitudinal plane (XY plane). Specimens for microstructural characterization were cut from the center and mechanically polished to a mirror finish with a 0.05-μm alumina suspension; then subjected to electrolytic polishing using a LectroPol-5 (Struers). The specimens were characterized with field-emission scanning electron microscopy (JEOL JSM-7600F) at an acceleration voltage of 15 kV with HKL Channel 5 software (Oxford Instruments). The same step size of 0.12 μm was used. The scanning area was 16×24 μm

for the EBSD orientation maps of group 1 and the 8th pass of group 2, and the others were $24 \times 24 \ \mu m$. However, misorientations below 3 deg were not considered during postprocessing.

Quantitative X-ray diffraction (XRD) measurements were performed with a Bruker D8 Advance X-ray diffractometer, which was equipped with a Cu target operating at 18 kW (50 kV × 360 mA). Scanning rate was 5 deg/min. The wave length λ is 0.15405 nm. The MDI Jade 5.0 software was used to evaluate XRD patterns, including the full width at half maximum (FWHM) and the peak maximum position. These data could approximately calculate the lattice strain and dislocation density.

Tensile tests and microhardness measurements were also performed on specimens from both groups. Each specimen was axially cut (*i.e.*, on the XY side) and polished; then any burrs, sharp corners, and oxide layers were removed to obtain a standard dog-bone specimen of $4 \times 1 \times 1$ mm. The tensile machine was used at a speed of 0.5 mm/min. Microhardness was measured by Vickers indentation at a load of 100 g and a loading time of 5 seconds. To determine the hardness of each specimen, we took the average of five measurements.

The thermal stability of the IU-ECAP specimens was determined by annealing in a vacuum. The specimens from both groups after the 8th pass were annealed at various temperatures and times (isochronal annealing at 423 K, 448 K, 473 K, 498 K, and 523 K (150 °C, 175 °C, 200 °C, 225 °C, and 250 °C) for 30 minutes; isothermal annealing at 423 K (150 °C) for 30, 60, 90, 120, and 150 minutes). The heating rate was 3-5 K/min. After annealing each sample, its microhardness was measured.

III. RESULTS AND DISCUSSION

A. *Extrusion Force*

Figure 4(a) shows the trend of extrusion force during the tests. For group 1, the extrusion force is the maximum value of each pass; while for group 2, the extrusion force is the maximum value when the ultrasonic vibration works. The extrusion force of group 1 increases slowly over the first four passes and reaches a maximum of 9460 N on the 4th pass; it then decreases during the 5th pass, stabilizes, and then increases again on the 8th pass. In group 2, the extrusion force gradually falls to a minimum of 5821.5 N over the 1st to 6th pass, then rises over the 7th and 8th passes.

For comparison, IU-ECAP significantly reduced the extrusion force. Over the 1st to 8th pass, the extrusion forces of group 2 decreased by 9.0, 15.5, 22.1, 30.3, 27.1, 32.3, 21.0, and 19.3 pct, respectively. The average value during the eight passes declined by 22.1 pct.

Figure 4(b) shows the load and deformation curves of the specimens on the 8th pass from groups 1 and 2, respectively, revealing significant differences between them. The extrusion force in group 2 was 19.3 pct lower than that in group 1. A curve similar to a square wave appears in Figure 4(b) because the ultrasonic exposure was suspended for 4 seconds after every 4 seconds of

exposure. Figure 4(c) shows a magnified part of the ultrasonic working curve in Figure 4(b); the load fell quickly from A to B and changed slowly to C when the ultrasonic vibration was restarted. The load then increased rapidly from C to D and changed slowly to E after 4 seconds. Thus, section ABC was caused by the combined ultrasonic vibration and loading. Note that the load of point B is defined as the extrusion force of the 8th pass, while section CDE is produced by loading without ultrasonic vibration; repeated in this way, it is clear that square waves occur with alternating stress cycles.

B. *Temperature*

Figure 5(a) and (b) shows the die temperature of groups 1 and 2 at three different time of a single extrusion pass, respectively. For the temperature test, the results were consistent with the tests performed in the two locations (holes 1 and 2). For group 1, the die had little temperature changes at three different time, the temperature kept about 295 K (22 °C). For group 2, the die temperature increased during extrusion process. Besides, the temperature changed similar to square wave according to the record in the middle of extrusion. The curve shows that the temperature fell quickly from A to B and rose gradually to C when the ultrasonic vibration was suspended. Since the ultrasonic was turned off at this time, the temperature rise was mainly due to the following reasons: first, the temperature of processed specimen in the pressing channel was much higher than that of the die; second, the transferred heat from the specimen caused the die temperature rise. The temperature then increased rapidly from C to D and rose slowly to E when the ultrasonic vibration was restarted. The die temperature reached 357 K (84 °C) at the end of extrusion. After that it decreased linearly, and the die temperature may drop to the room temperature before the next pass began.

In order to calculate the temperature of the specimen at the end of extrusion, the model can be simplified as a balance system based on the two points as follows. First, the heat (Q_1) released by the specimen equals to the heat (Q_2) absorbed by a boss with an inner diameter of 3 mm and outer diameter of 4.6 mm and length of 10 mm (see Figure 5(c)). Second, the boss temperature is stable at the end of the extrusion. Therefore, the heat can be calculated by the following equation:

$$Q_1 = C_1 M_1 \Delta T_1 \qquad [1]$$

$$Q_2 = C_2 M_2 \Delta T_2, \qquad [2]$$

where C_1 and C_2 are the specific heat capacity, C_1 is 385 J/(kg K) for copper and C_2 is 442 J/(kg K) for SKD11. M_1 and M_2 are the mass, for a specimen, M_1 could be calculated based on a diameter of 3 mm and length of 10 mm. For the boss, M_2 could approximately be evaluated. ΔT_1 and ΔT_2 are the temperature change, for the boss, ΔT_2 is 62 K, while for a specimen, because Q_1
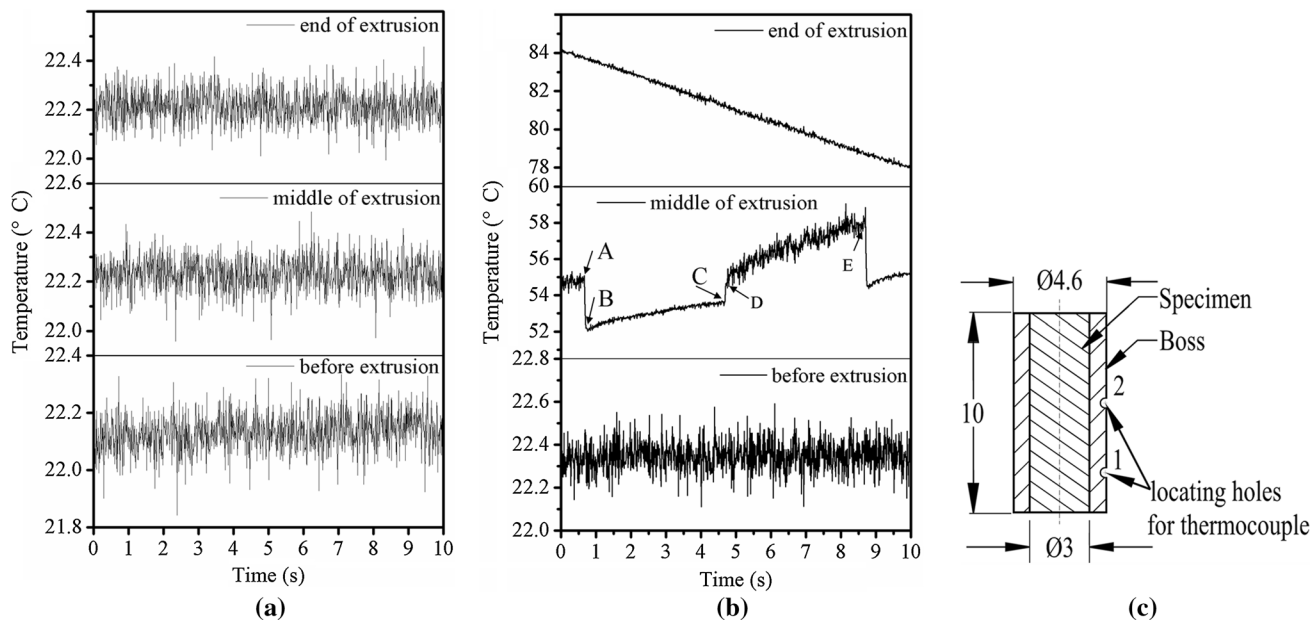
Fig. 5—Temperature measurement of the two groups: (a) Temperature measurement of group 1, (b) temperature measurement of group 2, (c) the simplified model.

equals to Q_2, ΔT_1 can be calculated by the following equation:

$$\Delta T_1 = C_2 M_2 \Delta T_2 / (C_1 M_1), \qquad [3]$$

where ΔT_1 equals to that the temperature of a specimen at the end of extrusion (T_1) subtracts 295 K (22 °C). The result shows T_1 is 385 K (112 °C). Thus, the temperature of specimens in the group 2 reached about 385 K (112 °C) at the end of extrusion. Compared with ECAP, the heat of IU-ECAP can promote the occurrence of the dynamic recrystallization.

C. Microstructure

Figure 6 shows the specimen microstructures of both groups after the 8th pass. The grain size distribution was heterogeneous, as reported by others[24–29]; the black line represents the high-angle grain boundaries (HAGBs) with misorientation angles larger than 15 deg, whereas the white line represents the low-angle grain boundaries (LAGBs) with misorientation angles of 3-15 deg. Higuera-Cobos et al.[28] revealed that in a severely deformed material with a large fraction of high-angle boundaries, there is virtually no need for thermal activation of nucleation because the boundaries can be easily moved. Thus, the dynamic recrystallization temperature of severely deformed copper is very close to room temperature.

For the as-received copper, the average grain size is ~15 μm. After the 8th pass of ECAP in group 1, the average grain size was refined to 0.51 μm (Figure 6(a)), while for IU-ECAP in group 2, the grain size was refined to 0.48 μm (Figure 6(b)). In addition, the specimen after IU-ECAP in group 2 showed a more homogeneous microstructure (Figure 6(b)), which is supported by Figure 6(c). Figure 6(c) shows that some grains in group

1 are larger than 2.0 μm and that the 0.35-μm grains account for the most scanning area, 18.47 pct, while no grain in group 2 is larger than 2.0 μm and most 0.45-μm grains account for the most scanning area, 18.77 pct.

Figure 6(d) shows the misorientation angles of groups 1 and 2 after the 8th pass. HAGBs in group 1 made up 55.3 pct of the grain boundaries, which agrees with the conclusion of Higuera-Cobos et al.[28]: in ECAP-processed copper, HAGBs likely comprise a maximum of 70 pct of grain boundaries. While that of group 2 was composed of 62.6 pct HAGBs, an increase of 7.3 pct compared with group 1.

Figure 6(e) and (f) shows the distribution of the dynamic recrystallized grains and subgrains after the 8th pass of ECAP and IU-ECAP, respectively. The yellow regions represented subgrains, surrounded by LAGBs. Besides, the software took each grain and measured the internal average misorientation angle within the grain, the average angle of subgrains was less than 3 deg. The red regions represented deformed grains, if the average angle in a grain exceeded the user-defined minimum angle to define a subgrain, (3 deg), the grain was classified as being "deformed" and all the remaining grains were classified as recrystallized, the blue regions represented dynamic recrystallized grains. In group 1, the blue and yellow grains account for 2.8 and 18.15 pct of the scanning area, respectively, while in group 2, these values were 5.7 pct and 23.97 pct, respectively. Thus, the dynamic recrystallization fraction of group 2 was more than twice that of group 1, and the subgrain fraction of group 2 increased by 5.82 pct over group 1.

To further compare the characteristics of ECAP and IU-ECAP processes, EBSD was also performed on the specimens from the two groups after the 4th and 6th passes. Figure 7 shows the specimen microstructures of group 1 after 4th and 6th passes. Figure 8 shows the
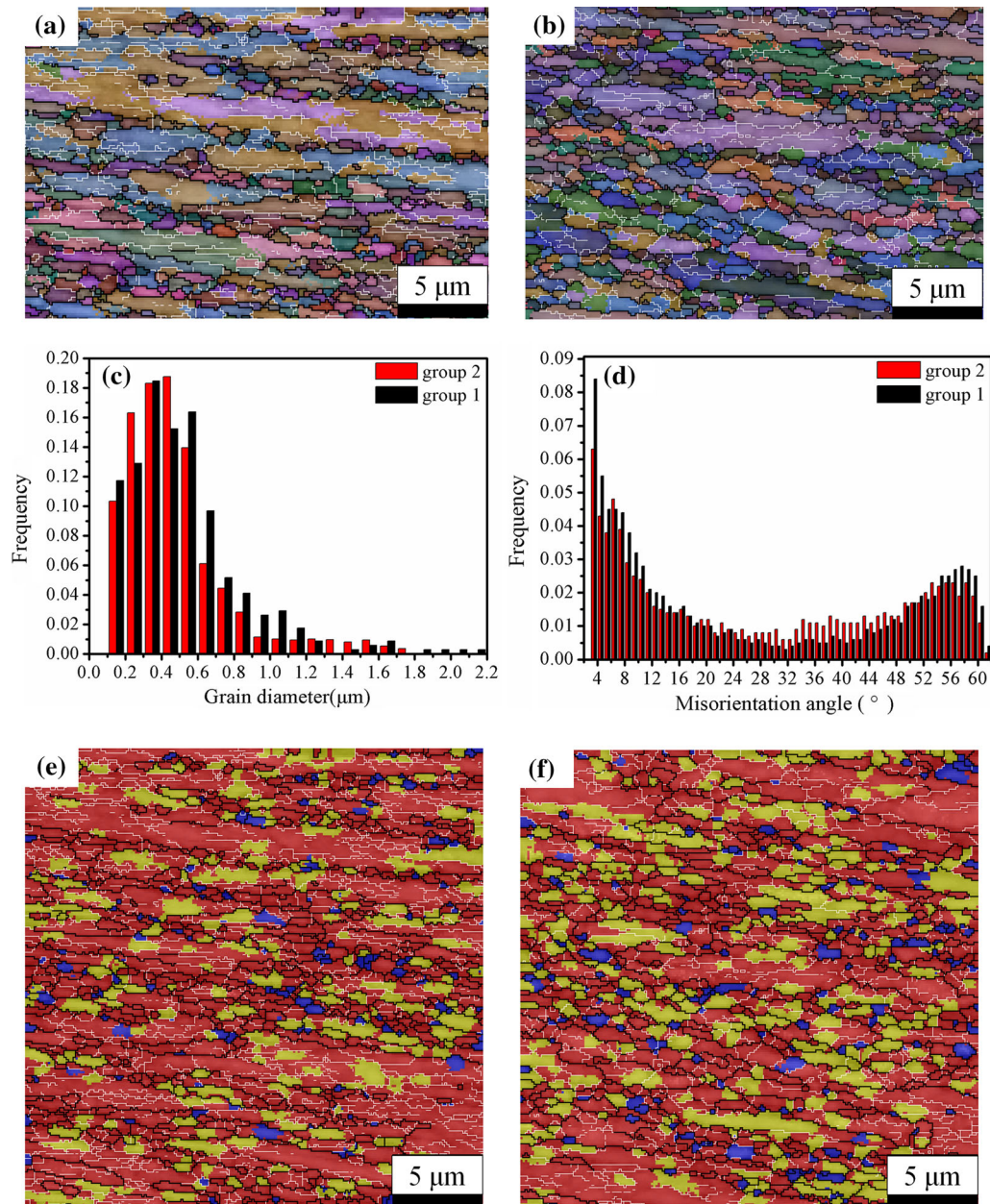
Fig. 6—Microstructure after the 8th pass: (*a*) orientation map of group 1, (*b*) orientation map of group 2, (*c*) grain size of the two groups, (*d*) misorientation angle of the two groups, (*e*) dynamic recrystallization and subgrain of group 1, (*f*) dynamic recrystallization and subgrain of group 2.

specimen microstructures of group 2 after 4th and 6th passes.

Table II summarizes the average grain sizes, HAGBs, subgrain fractions, and dynamic recrystallization fractions during ECAP and IU-ECAP after the 4th, 6th, and 8th passes for comparison. After the 4th, 6th, and 8th passes, the average grain sizes of IU-E-CAP decreased by 14.7, 13.9, and 5.9 pct, respectively; HAGBs of IU-ECAP increased by 26.2, 16.7, and 7.3 pct, respectively; the dynamic recrystallization fractions of IU-ECAP increased by 0.25, 0.275, and 2.9 pct, respectively; the subgrain fractions of IU-ECAP increased by 11.43, 14.46, and 5.82 pct, respectively. Furthermore, compared with Figures 7(b) and 8(b)

shows a more homogeneous microstructure. All these data revealed that the ultrasonic vibration decreased the grain size and formed a more homogeneous microstructure.

The microstructure of ultrafine-grained copper processed by IU-ECAP changed as follows: after the 8th pass, the grains had refined from 15 to 0.48 μm. The fraction of dynamic recrystallized grains increased as the number of passes increased owing to the thermal effect of ultrasonic vibration. As shown in Figures 6(f) and 8(c) and (d), the size of the recrystallized grains remains at the same level as the ultrafine grains. The fraction of subgrains grew from the 4th to the 6th pass, however the fraction declined after the 8th pass. The area ratio of the
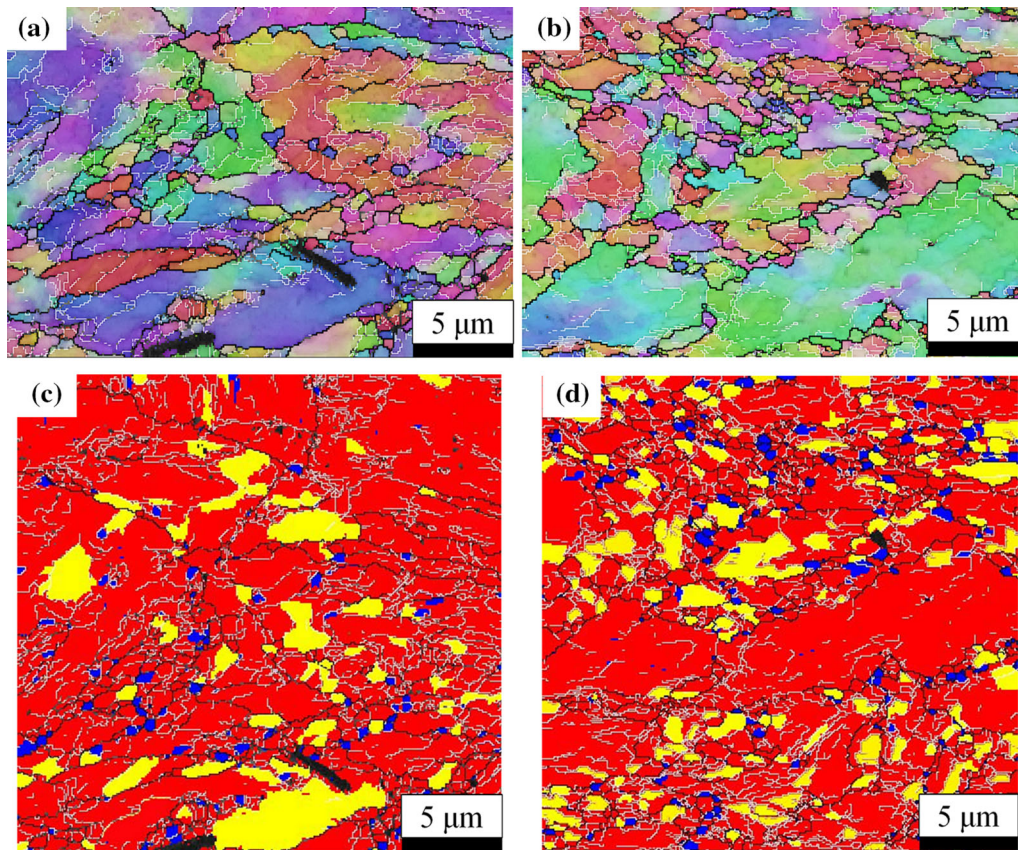
Fig. 7—Microstructures in group 1 after the 4th and 6th passes: (a) orientation map after 4th pass, (b) orientation map after 6th pass, (c) recrystallization and subgrain after the 4th pass, (d) recrystallization and subgrain after the 6th pass.

subgrains after the 4th pass was 22.63 pct, which is more than that of group 1 after the 8th pass. Clearly, as the subgrain fraction increased, so did the sub-boundary fraction. A low-angle boundary or sub-boundary can be represented by an array of dislocations,[29] and the sub-boundary fraction reflects the dislocation density. Thus, we infer that the dislocation density of specimens in group 2 after the 4th pass was higher than that of group 1 after the 8th pass.

During the grain refinement in ECAP, the dislocation density increased as the strain increased. These dislocations accumulated in some regions and formed dislocation cells. These dislocation cells changed into LAGBs or HAGBs, and then the elongated grains were refined into small grains and subgrains.[4,30–32] While during the grain refinement in IU-ECAP, the strain increased more rapidly under the joint action of ultrasonic vibration and loading. This produced denser dislocations and more dislocation cells. Finally, smaller grains and more subgrains were produced. Simultaneously, the thermal effect of ultrasonic vibration could lead to dynamic recrystallization of subgrains as the number of passes increased, the LAGBs grow continuously and up to HAGBs finally. The subgrains transform to real grains, resulting in the homogeneity of the microstructure. This may be the reason why the fraction of subgrains

decreased to 23.97 pct while the fraction of recrystallized grain increased to 5.7 pct after the 8th pass in group 2.

D. Dislocation Density

Figure 9(a) shows the magnified XRD patterns of the different crystal planes from as-received copper and groups 1 and 2. The intensity of the XRD pattern could be compared, XRD patterns indicated the as-received copper had the largest intensity and the smallest FWHM values, while group 2 had the weakest intensity and the largest FWHM values. Youssef et al.[33] reported that the refinement of grain size and the introduction of lattice strain could cause the XRD peaks to broaden and decrease their intensities. The FWHM analysis was used to approximately calculate the lattice microstrain from the XRD line broadening.[34] This analysis presumes that crystallite size broadening and strain-broadening profiles can be approximated by Cauchy and Gaussian functions, respectively, leading to the following equation[33,34]:

$$\frac{(\delta 2\theta)^2}{\tan^2 \theta_0} = \frac{\lambda}{d}\left(\frac{\delta 2\theta}{\tan \theta_0 \sin \theta_0}\right) + 25, \qquad [4]$$

where $\delta 2\theta$ is the measured FWHM, θ_0 is the peak maximum position, λ is the wave length, d is the average
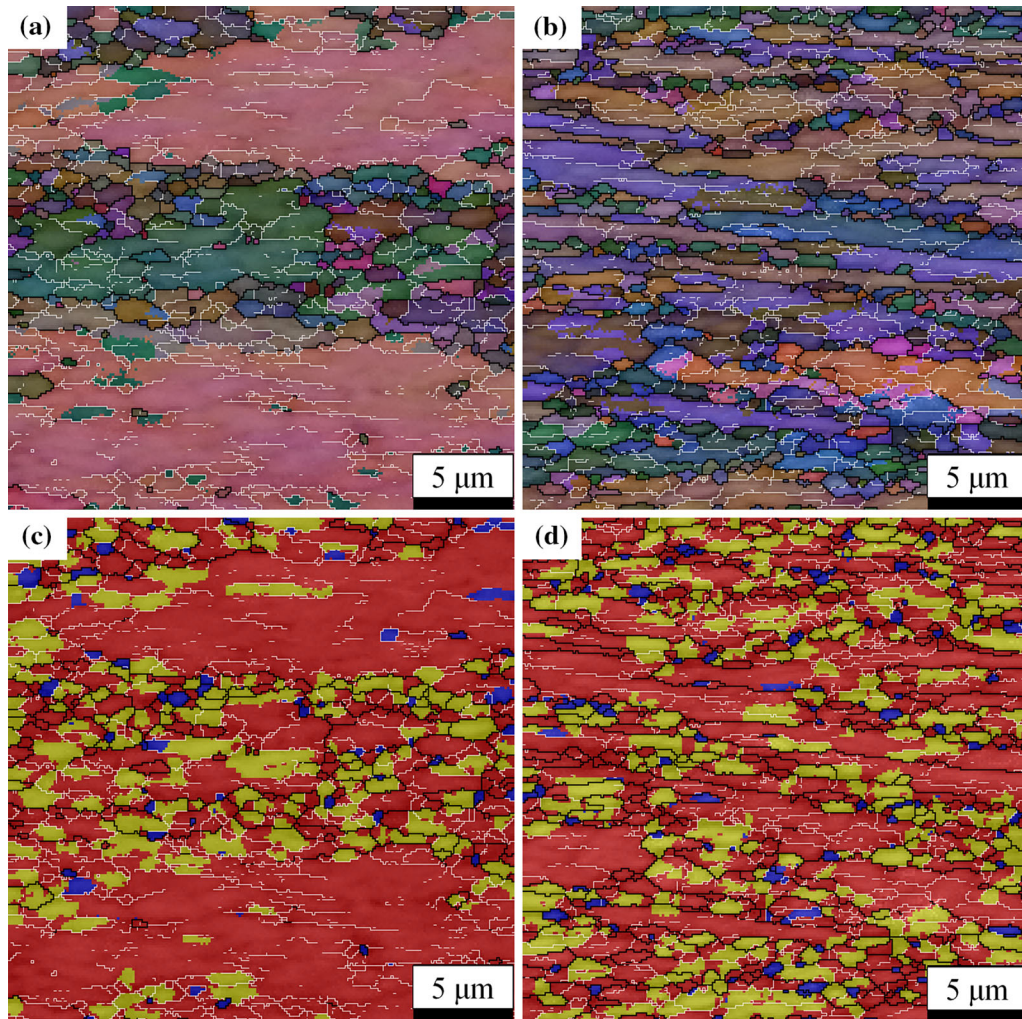
Fig. 8—Microstructures in group 2 after the 4th and 6th passes: (*a*) orientation map after 4th pass, (*b*) orientation map after 6th pass, (*c*) recrystallization and subgrain after the 4th pass, (*d*) recrystallization and subgrain after the 6th pass.

Table II. Microstructures in the Two Groups After the 4th, 6th, and 8th Passes

Pass	Grain Diameter (μm)	HAGB (Pct)	Dynamic Recrystallized-grain (Pct)	Subgrains (Pct)
4 (group1)	0.95	29.3	2.10	11.2
4 (group2)	0.81	55.5	2.35	22.63
6 (group1)	0.79	43.8	2.51	12.9
6 (group2)	0.68	60.5	2.785	27.36
8 (group1)	0.51	55.3	2.8	18.15
8 (group2)	0.48	62.6	5.7	23.97

crystallite size, and *e* is the lattice strain. For all measured peaks of the specimens, the $(\delta 2\theta)^2 / \tan^2 \theta_0$ against $(\delta 2\theta)/(\tan \theta_0 \sin \theta_0)$ could be fitted to calculate the lattice strain. Figure 9(b) shows how the lattice strain changed in the two groups, the zero pass represented the as-received copper. Compared with group 1, group 2 had the bigger lattice strain at the same pass.

For the materials subjected to severe plastic deformation, dislocations density ρ can be represented in terms of the average crystallite size *d* and the lattice strain *e*, leading to the following equation[35]:

$$\rho = 2\sqrt{3}\langle e^2 \rangle^{1/2} \big/ (d \times b),$$ [5]

where *b* is the Burgers vector (2.56×10^{-10} m for Cu). The calculated ρ in groups 1 and 2 are shown in Figure 9(c), which indicated that the as-received copper
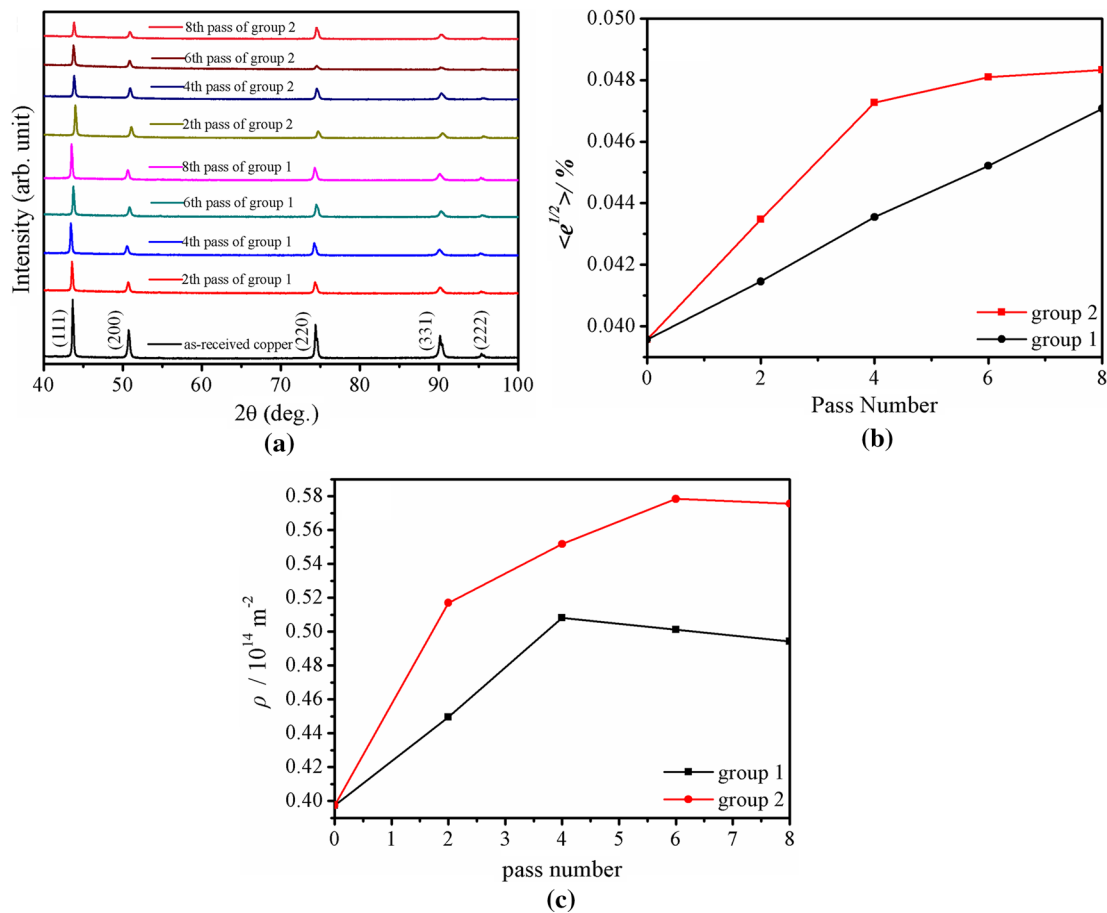
Fig. 9—X-ray diffraction (XRD) analysis. (*a*) XRD patterns of as-received copper and the two groups, (*b*) lattice strain of the two groups, (*c*) dislocation density of the two groups.

had the weakest dislocations density, while group 2 had the largest values. For group 1, the dislocation density saturated after four passes, reaching 0.508286×10^{14} m^{-2}. For group 2, the dislocation density saturated after six passes, reaching 0.578408×10^{14} m^{-2}. X-ray diffraction (XRD) analysis revealed that IU-ECAP increased the dislocation density of specimens.

E. *Mechanical Properties*

Figure 10(a) shows the ultimate tensile stress (UTS) of both groups from the 1st to the 8th pass obtained by tensile test. The zero pass represented the as-received copper. The UTS gradually increased in both groups, and the maximum UTS was higher in group 2 than in group 1 after the 4th, 5th, 6th, 7th, and 8th passes.

Figure 10(b) shows the microhardness of the specimens from both groups, and the original microhardness is 114 HV. The microhardness of group 1 increased after the 1st pass but saturated after four passes, reaching 127 HV after eight passes. In group 2, the microhardness saturated after six passes, reaching 133 HV after eight passes. Across the 1st pass to the 8th pass, the specimen in group 2 had higher microhardness than group 1. The difference in microhardness was minimal before the 5th pass, but it increased with more passes. This is consistent with the previous analysis. It is the rising dislocation density and smaller grain that make group 2 have a microhardness higher than group 1.

F. *Thermal Stability*

Figure 11(a) shows the microhardness of specimens from both groups after the 8th pass for various annealing temperatures. As the annealing temperature increased, the microhardness decreased. The microhardness of group 1 decreased from 127 to 62 HV when the annealing temperature increased from 423 K to 473 K (150 °C to 200 °C). For group 2, the microhardness decreased from 133 to 60 HV when the annealing temperature increased from 473 K to 523 K (200 °C to 250 °C).

Figure 11(b) shows how the microhardness changed in both groups after the 8th pass with various annealing times. In the figure, the error function curves, which are known to represent the behavior of static recrystallization,[29] are fitted to the measured microhardness values. Over the given temperature range, group 1 showed much faster static recrystallization than group 2. In group 1, the microhardness had decreased by 50 pct at ~52 minutes, but in group 2, the same reduction occurred at ~81 minutes.

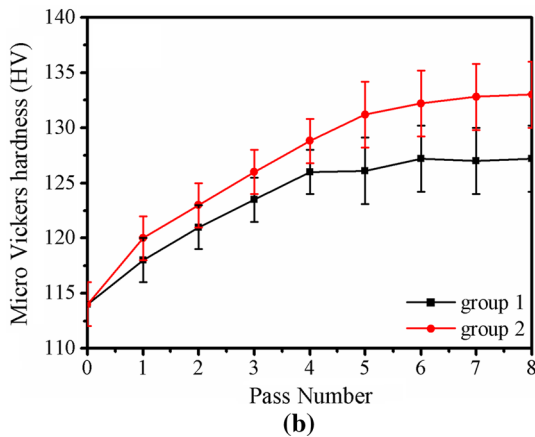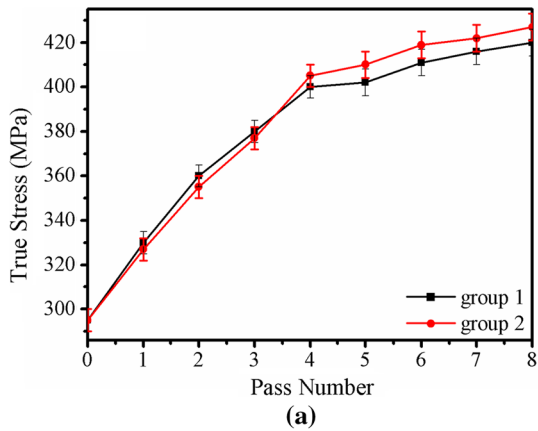Cao *et al.*[36] reported that a microstructure's thermal stability can be defined as its resistance to recovery and

Fig. 10—Mechanical test: (*a*) true stress of the two groups, (*b*) micro-hardness as a function of pass number.

Fig. 11—Thermal stability: (*a*) isochronal annealing for 30 min, (*b*) isothermal annealing at 423 K (150°C).

recrystallization, which can be quantified by either the time to 50 pct recrystallization (in an isothermal experiment) or the temperature at which 50 pct recrystallization occurs (in a continuous heating or an isochronal experiment). Increases in the time or temperature to recrystallize the microstructure are a result of greater thermal stability.

Conventional ECAP has been shown in many studies to produce specimens with poor thermal stability.[26,36,37] Based on annealing experiments, group 2 had better thermal stability than group 1. In short, static recrystallization occurred at a higher temperature or after a longer time in group 2 than in group 1.

IV. CONCLUSIONS

Compared with conventional ECAP, intermittent ultrasonic-assisted ECAP can impose cyclic square-wave force, which is a flexible and reliable way to produce ultrafine-grained copper. Main conclusions are summarized as follows:

(1) IU-ECAP significantly reduced the extrusion force by 22.1 pct. The thermal effect of ultrasonic vibration is a key factor during IU-ECAP. IU-E-CAP controls the temperature rise by adjusting the ultrasonic exposure time.
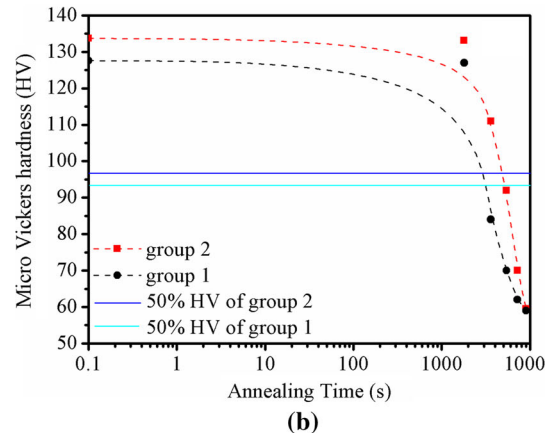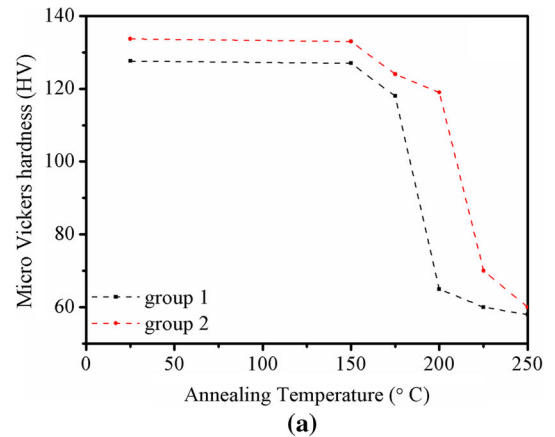
(2) Temperature test showed that the die of ECAP had little temperature changes, while the die temperature of IU-ECAP changed similar to square wave during extrusion process. IU-ECAP could control the thermal effect of ultrasonic vibration effectively. The die temperature of IU-ECAP reached 357 K (84 °C) at the end of extrusion. The specimen temperature of IU-E-CAP reached about 385 K (112 °C). The heat could promote the occurrence of the dynamic recrystallization.

(3) The average grain sizes of the two groups reached the level of ultrafine grains after the 4th pass. While compared with ECAP, the average grain sizes of IU-ECAP decreased by 14.7, 13.9, and 5.9 pct after the 4th, 6th, and 8th passes, respectively. In addition, IU-ECAP formed a more homogeneous microstructure. IU-ECAP promoted conversion from LAGBs to HAGBs, and increased the fractions of subgrains and dynamic recrystallized grains.

(4) The microhardness and UTS of the IU-ECAP specimen were higher than those of the ECAP ones, because IU-ECAP generated a higher dislocation density and smaller grains.

(5) XRD analysis showed that the specimen of IU-ECAP had the weakest intensity and the

largest FWHM value. Theoretical calculation showed IU-ECAP increased the lattice strain and the dislocation density of specimen.

(6) The annealing experiments showed that IU-ECAP was also superior to ECAP in terms of thermal stability. The specimens processed by IU-ECAP exhibited static recrystallization at a higher temperature or a longer duration.

ACKNOWLEDGMENTS

REFERENCES

1. N.J. Petch: *J. Iron. Steel. Inst.*, 1963, vol. 174, pp. 25–28.
2. E.O. Hall: *Proc Phys. Soc.*, 1951, vol. 643, pp. 747–52.
3. V.M. Segal: *Mater. Sci. Eng. A*, 1995, vol. 197, pp. 157–64.
4. R.Z. Valiev and T.G. Langdon: *Prog. Mater. Sci.*, 2006, vol. 51, pp. 881–981.
5. T.G. Langdon: *J. Mater. Sci.*, 2007, vol. 42, pp. 3388–97.
6. P.R. Cetlin, M.T.P. Aguilar, R.B. Figueiredo, and T.G. Langdon: *J. Mater. Sci.*, 2010, vol. 45, pp. 4561–70.
7. O. Nejadseyfi, A. Shokuhfar, A. Azimi, and M. Shamsborhan: *J. Mater. Sci.*, 2015, vol. 50, pp. 1513–22.
8. R.Y. Lapovok: *J. Mater. Sci.*, 2005, vol. 40, pp. 341–46.
9. A.P. Zhilyaev and T.G. Langdon: *J. Mater. Sci.*, 2012, vol. 47, pp. 7888–93.
10. V.V. Stolyarov, Y.T. Zhu, I.V. Alexandrov, T.C. Lowe, and R.Z. Valiev: *Mater. Sci. Eng. A*, 2001, vol. 299, pp. 59–67.
11. V.V. Stolyarov, Y.T. Zhu, I.V. Alexandrov, T.C. Lowe, and R.Z. Valiev: *Mater. Sci. Eng. A*, 2003, vol. 343, pp. 43–50.
12. H.S. Dong, B.C. Kim, K.T. Park, and W.Y. Choo: *Acta Mater.*, 2000, vol. 48, pp. 3245–52.
13. H.S. Dong, B.C. Kim, Y.S. Kim, and K.T. Park: *Acta Mater.*, 2000, vol. 48, pp. 2247–55.
14. K. Neishi, Z. Horita, and T.G. Langdon: *Mater. Sci. Eng. A*, 2002, vol. 325, pp. 54–58.
15. A.P. Zhilyaev, B.K. Kim, J.A. Szpunar, M.D. Baró, and T.G. Langdon: *Mater. Sci. Eng. A*, 2005, vol. 391, pp. 377–89.
16. Z. Huang, M. Lucas, and M.J. Adams: *Ultrasonics*, 2002, vol. 40, pp. 43–48.
17. Y. Liu, S. Suslov, Q. Han, L. Hua, and C. Xu: *Metall. Mater. Trans. A*, 2013, vol. 44A, pp. 3232–44.
18. D. Pal and B. Stucker: *J. Appl. Phys.*, 2013, vol. 113, pp. 203517–18.
19. J.F. Zhang, F.Z. Xuan, and Y.X. Xiang: *Epl*, 2013, vol. 103, pp. 613–16.
20. F. Ahmadi, M. Farzin, M. Meratian, S.M. Loeian, and M.R. Forouzan: *Int. J. Adv. Manuf. Tech.*, 2015, vol. 79, pp. 503–12.
21. F. Djavanroodi, H. Ahmadian, K. Koohkan, and R. Naseri: *Ultrasonics*, 2013, vol. 53, pp. 1089–96.
22. F. Ahmadi, M. Farzin, and M. Mandegari: *Ultrasonics*, 2015, vol. 63, pp. 111–17.
23. Y. Iwahashi, J. Wang, Z. Horita, M. Nemoto, and T.G. Langdon: *Scr. Mater.*, 1996, vol. 35, pp. 143–46.
24. C.F. Gu and C.H.J. Davies: *Mater. Sci. Eng. A*, 2010, vol. 527, pp. 1791–99.
25. A. Godfrey and Q. Liu: *Scr. Mater.*, 2009, vol. 60, pp. 1050–55.
26. X. Molodova, G. Gottstein, M. Winning, and R.J. Hellmig: *Mater. Sci. Eng. A*, 2007, vol. 460, pp. 204–13.
27. N. Lugo, N. Llorca, J.J. Sunol, and J.M. Cabrera: *J. Mater. Sci.*, 2010, vol. 45, pp. 2264–73.
28. O.F. Higuera-Cobos and J.M. Cabrera: *Mater. Sci. Eng. A*, 2013, vol. 571, pp. 103–14.
29. F.J. Humphreys and M. Hatherly: *Recrystallization and Related Annealing Phenomena*, 2nd ed., Elsevier, New York, 2004.
30. Y.M. Wang and E. Ma: *Acta Mater.*, 2004, vol. 52, pp. 1699–09.
31. B. Bay, N. Hansen, D.A. Hughes, and D. Kuhlmann-Wilsdorf: *Acta Metall. Mater.*, 1992, vol. 40, pp. 205–19.
32. X. Zhang, L. Hua, and Y. Liu: *Mater. Sci. Eng. A*, 2012, vol. 535, pp. 153–63.
33. K.M. Youssef, R.O. Scattergood, K.L. Murty, and C.C. Koch: *Scr. Mater.*, 2006, vol. 54, pp. 251–56.
34. H.P. Klug and L. Alexander: *X-Ray Diffraction Procedures for Polycrystalline and Amorphous Materials*. Wiley, New York, 1974.
35. G.K. Williamson and R.E. Smallman: *Philos. Mag.*, 1956, vol. 1, pp. 34–36.
36. W.G. Cao, C.F. Gu, E.V. Pereloma, and C.H.J. Davies: *Mater. Sci. Eng. A*, 2008, vol. 492, pp. 74–79.
37. P.K. Jayakumar, K. Balasubramanian, and G.R. Tagore: *Mater. Sci. Eng. A*, 2012, vol. 538, pp. 7–13.